

# Frequency and mode identification of $\gamma$ Doradus from photometric and spectroscopic observations<sup>\*</sup>

E. Brunsden<sup>1,2,†</sup>, K. R. Pollard<sup>2</sup>, D. J. Wright<sup>3</sup>, P. De Cat<sup>4</sup>, P. L. Cottrell<sup>5</sup>

<sup>1</sup>*Department of Physics, University of York, Heslington, York, YO10 5DD, UK*

<sup>2</sup>*Department of Physics and Astronomy, University of Canterbury, Private Bag 4800, Christchurch, New Zealand*

<sup>3</sup>*Department of Astrophysics, University of New South Wales, Sydney, NSW 2052 Australia*

<sup>4</sup>*Royal Observatory of Belgium, Ringlaan 3, 1180 Brussel, Belgium*

<sup>5</sup>*Monash Centre for Astrophysics, School of Physics and Astronomy, Monash University, Victoria 3800, Australia*

## ABSTRACT

The prototype star for the  $\gamma$  Doradus class of pulsating variables was studied employing photometric and spectroscopic observations to determine the frequencies and modes of pulsation. The four frequencies found are self-consistent between the observation types and almost identical to those found in previous studies (1.3641 d<sup>-1</sup>, 1.8783 d<sup>-1</sup>, 1.4742 d<sup>-1</sup> and 1.3209 d<sup>-1</sup>). Three of the frequencies are classified as  $l, m = (1, 1)$  pulsations and the other is ambiguous between  $l, m = (2, 0)$  and  $(2, -2)$  modes. Two frequencies are shown to be stable over twenty years since their first identification. The agreement in ground-based work makes this star an excellent calibrator between high-precision photometry and spectroscopy with the upcoming TESS observations and a potential standard for continued asteroseismic modelling.

**Key words:** line: profiles, techniques: spectroscopic, Gamma Doradus, stars: variables: general, stars: oscillations

## 1 INTRODUCTION

Stars showing g-mode pulsations, such as  $\gamma$  Doradus ( $\gamma$  Dor) stars are important targets for asteroseismic investigation. Revealing the interior of stars through the determination of properties such as convection, opacity, rotation, and ionization has profound impacts on our understanding of stellar evolution. The  $\gamma$  Dor stars are a key class where the high-order non-radial g-mode pulsations propagate deep into the star, allowing us to probe large regions of their interior.

The excitation mechanism for  $\gamma$  Dor stars is explained by convective flux blocking (Guzik et al. 2000; Dupret et al. 2005), although turbulent convection has also been considered as an excitation of oscillations (Grassitelli et al. 2015; Xiong et al. 2016).

The class has a localised position on the Hertzsprung-Russell diagram, on or near the main sequence at the red edge of the classical instability strip, which gives each  $\gamma$  Dor star a similar overall structure.  $\gamma$  Dor stars are found in the transition region from convective cores and radiative en-

velopes to radiative cores and convective envelopes, making them useful tools for probing this boundary to improve theoretical modelling. Intensive efforts are being made to understand  $\gamma$  Dor asteroseismology and to determine their internal conditions, such as the sizes of their convection zones and their internal rotation rates (some recent examples include Bedding et al., (2015), Van Reeth et al., (2016), Schmid & Aerts, (2016)).

Mode identifications of  $\gamma$  Dor stars are required to provide inputs and to test theoretical stellar models. The list of  $\gamma$  Dor stars with partial or complete mode identifications for even one frequency is short (only around eight stars with full geometric mode identifications having been published to date). Precision photometric methods still generally lack spectroscopic verification and in some cases show stark disagreement (e.g. Uytterhoeven et al., 2008, Brunsden et al., 2015). Using both photometric and spectroscopic data in a complementary way allows us to test our frequency and mode identification methods.

The prototype star of the class,  $\gamma$  Doradus itself (HD 27290, HR 1338, HIP 19893) is a bright ( $V = 4.20$ ), F1 V (Gray et al. 2006) star which has been observed for many decades as a known variable. It was defined as the class prototype in 1999 (Kaye et al. 1999). This paper details the analysis of extensive sets of photometric and spectroscopic data obtained over a 20 year period. Section 2 outlines these data and section 3 their treatment. Section 4 and Section 5

<sup>\*</sup> This paper includes data taken at the University of Canterbury Mount John Observatory, New Zealand, the Sutherland South African Astronomical Observatory (SAAO), Cape Town Observatory operated by SAAO and Cerro Tololo Inter-American Observatory, Chile.  
<sup>†</sup> E-mail: emily.brunsdan@gmail.com

**Table 1.** Stellar parameters found for  $\gamma$  Doradus in previous studies. Entries with  $\star$  are values from spectroscopy and entries with  $\dagger$  are from Strömgren photometry.

$T_{\text{eff}}$	$\log g$	$v \sin i$ ( $\text{km s}^{-1}$ )	Ref
7164		$59.5 \pm 3$	Ammeler-von Eiff & Reiners (2012) $\star$
7060	3.97		Gray et al. (2006) $\star$
7120	4.25		Dupret et al. (2005) $\dagger$
7202	4.23		Dupret et al. (2005) $\dagger$
		62	Kaye et al. (1999) $\star$
7180			Sokolov (1995) $\star$

describe the frequency and mode identification. A discussion of all the results and a concluding statement is found in Section 6 and Section 7, respectively.

## 2 OBSERVATIONS

One of the most studied  $\gamma$  Dor class members, new observations are presented here of the prototype star. Stellar parameters have been previously measured for  $\gamma$  Doradus. Restricting reports to results no older than 1995, Table 1 lists recent values found for  $T_{\text{eff}}$ ,  $\log g$  and  $v \sin i$ . The results show consistent findings for  $T_{\text{eff}}$  of around 7150 K and  $\log g$  near 4.1. These values are typical for  $\gamma$  Dor group members (see, for example, Kahraman Aliçavuş et al., 2017).

$\gamma$  Doradus has been a known variable star since observations by Cousins (1960) and Cousins & Warren (1963). A summary of the frequencies previously found in  $\gamma$  Doradus is given in Table 2. The first periods were found in Strömgren photometry and published in Cousins (1992) and confirmed in Balona et al. (1994b) also using Strömgren photometry. Further observations using multi-site Strömgren and Johnson filter photometry again supported these periods and found evidence for a third (Balona et al. 1994a). In multi-site spectroscopy analysed in the same study,  $f_{11}$  and  $f_{12}$  were detected in the radial velocity measurements. Mode identification from the spectroscopic line profile variations (Balona 1986a,b, 1987) classified  $f_{11}$ ,  $f_{12}$  and  $f_{13}$  as  $(l, m) = (3, 3)$ ,  $(1, 1)$  and  $(1, 1)$  respectively (Balona et al. 1996). These modes were found with an inclination of  $70^\circ$ . Modelling by Dupret et al. (2005) identified  $f_{11}$  and  $f_{12}$  to be both well-fitted by  $l = 1$  modes using time-dependent convection models on the photometric data. Observations with the Solar Mass Ejection Imager (SMEI) aboard the Coriolis satellite found the previously known  $f_{11}$ ,  $f_{12}$  and  $f_{13}$ , then further identified  $f_{14}$  and  $f_{15}$  (Tarrant et al. 2008). The authors also note the occurrence of a frequency at  $2.743 \text{ d}^{-1}$ , identifying it as a combination frequency of  $f_{12}$  and  $f_{15}$ .

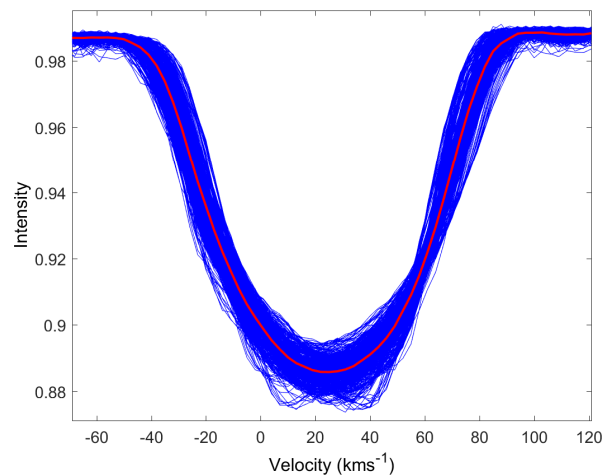
Photometric data were supplied by L. Balona and have been previously analysed for frequencies (Cousins 1992; Balona et al. 1994b,a, 1996). These data were taken at a variety of sites and in several photometric filters, the details of which are described in Table 3.

Spectra from the University of Canterbury Mt John Observatory (UCMJO) in New Zealand were collected using the 1m McLellan telescope with the fibre-fed High Efficiency and Resolution Canterbury University Large Echelle Spec-

**Table 2.** Previously identified frequencies in  $\gamma$  Doradus. The formal uncertainty in the last digit is displayed in parentheses.

ID	Phot. <sup>1</sup> ( $\text{d}^{-1}$ )	Phot. <sup>2</sup> ( $\text{d}^{-1}$ )	Phot. <sup>3</sup> ( $\text{d}^{-1}$ )	Spec. <sup>4</sup> ( $\text{d}^{-1}$ )	Phot. <sup>5</sup> ( $\text{d}^{-1}$ )
$f_{11}$	1.321	1.32099	1.32098 (2)	1.365 (2)	1.32093 (2)
$f_{12}$	1.364	1.36353	1.36354 (2)		1.36351 (2)
$f_{13}$			1.475 (1)		1.471 (1)
$f_{14}$					1.39 (5)
$f_{15}$					1.87 (3)

<sup>1</sup>Cousins (1992), <sup>2</sup>Balona et al. (1994b), <sup>3</sup>Balona et al. (1994a),  
<sup>4</sup>Balona et al. (1996), <sup>5</sup>Tarrant et al. (2008)

**Figure 1.** Line profiles of 613 observations of  $\gamma$  Doradus. The mean profile is over-plotted in red. This star shows large pulsational variation from observation to observation, particularly near the centre of the profile.

trograph (HERCULES) with a resolving power of  $R = 50000$  operating over a range of  $3800 \text{ \AA}$  to  $8000 \text{ \AA}$  (Hearnshaw et al. 2002). We observed  $\gamma$  Doradus over 15 months from June 2011 to August 2012 at UCMJO, during which time we obtained 625 observations. Typically we took 10 – 20 observations in a single night. The sampling of the data can be seen in the window function in Figure 2. We produced a total of 613 line profiles for analysis which show clear variation (Figure 1).

## 3 ANALYSIS METHODS

We performed time-series analysis using FAMIAS (Zima 2008), applied as in Zima et al. (2006) and in SIGSPEC (Reegen 2007). For spectroscopic data this entailed an analysis of the variations in the representative line profiles which identified the frequencies present. For photometric data, we analysed white light or multi-colour photometry for periodic signals.

The amplitude ratio method (Balona & Stobie 1979; Watson 1988; Cugier et al. 1994; Daszyńska-Daszkiewicz et al. 2002; Dupret et al. 2003) uses calculations of the ratios between the amplitudes and differences in phases of different

**Table 3.** Summary of photometric observations of  $\gamma$  Doradus with number of observations, dates, total time span ( $\Delta T$ ), filter sets used (with number of filters) and references to the original publications.

N of Obs.	Dates Observed	$\Delta T$ (days)	Filters (number)	Ref.
<b>suth</b> photometry				
447	Jan 1993-Nov 1994	693	Ström. (4)	<sup>1, 2, 3</sup>
175	Nov 1989-Mar 1990	132	John. V (1)	<sup>4</sup>
<b>cape</b> photometry				
167	Oct 1981-Mar 1991	3427	Ström. (4)	<sup>4</sup>
151	Dec 1993-Jan 1994	80	John. B V	<sup>2</sup>
			DDO 45,48 (4)	
<b>ctio</b> photometry				
400	Jan 1994-Nov 1994	325	John. V (1)	<sup>2, 3</sup>

<sup>1</sup>Balona et al. (1994b), <sup>2</sup>Balona et al. (1994a),

<sup>3</sup>Balona et al. (1996), <sup>4</sup>Cousins (1992).

filters in a multi-coloured photometric system to determine  $l$  values of the modes. Typically this method constrains the  $l$  values rather than giving unique solutions. We used the photometric analysis toolbox in FAMIAS (Zima 2008).

### 3.1 Delta Function Cross Correlation

To maximise the signal obtained from the line profile variations, we used a  $\delta$ -function cross-correlation technique. To prepare the normalised spectra, telluric regions and the broad hydrogen lines,  $H\alpha$ ,  $H\beta$  and  $H\gamma$ , are removed.

A line list is generated by Synspec (Hubeny & Lanz 2011), and from this list, very weak lines (equivalent widths less than 5.0 mÅ) are removed. Cross-correlation of the remaining lines (typically 2000 to 5000) is done using standard cross-correlation techniques and then using the  $\delta$ -function template. The scaled  $\delta$ -function cross-correlation technique (Wright, 2008, building on Wright et al., 2007) cross-correlates the spectra with a template of  $\delta$  functions at the correct wavelengths and line depths. Cross-correlation produces a representative spectral line, or zero-point line profile, for each of the observations. The cross-correlation process gives high signal-to-noise representative line profiles for the star.

The pixel-by-pixel method (Mantegazza 2000) is a line-profile variation method that looks at the movement of each individual pixel in a spectral absorption line and analyses them as a time series with the calculation of a Fourier spectrum. Each pixel is then used to create an average Fourier spectrum of the frequencies present in the line profile.

We used the Fourier spectra for the Pixel-by-Pixel (PBP) technique applied to the representative line profiles to identify frequencies. We then analysed these frequencies to determine mode identifications using the Fourier Parameter Fit method (Zima 2009).

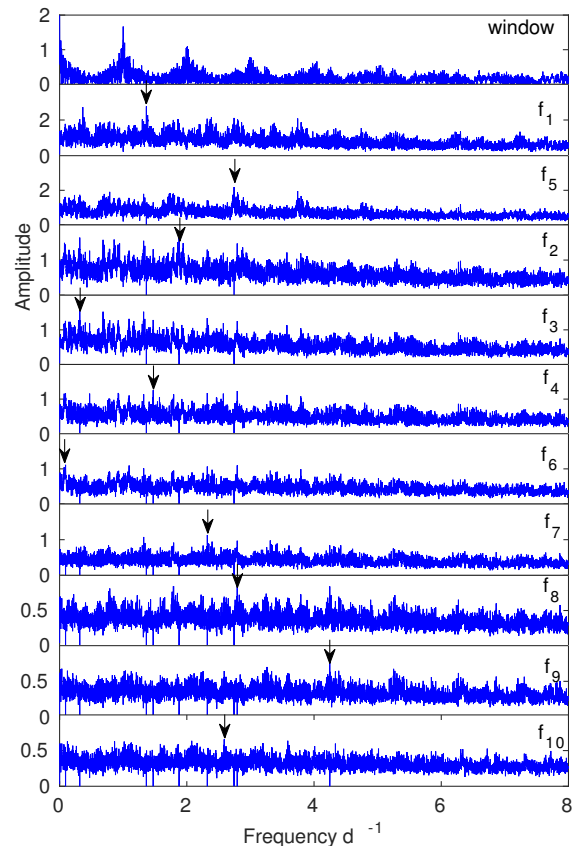


**Figure 2.** Fourier spectra showing the ten identified frequencies using the PBP technique. The top panel shows the spectral window which is representative of the data sampling.

## 4 FREQUENCY ANALYSIS

We performed frequency analysis on both spectroscopic and photometric data in FAMIAS and SigSpec. We restricted the analysis to frequencies within an extended  $\gamma$  Dor frequency range ( $0-8 \text{ d}^{-1}$ ) due to the absence of any higher-amplitude frequencies, which would be indicative of p-mode pulsation. One-day aliases and harmonics were identified and removed.

### 4.1 Spectroscopic Frequency Analysis

We identified ten candidate frequency peaks in the PBP Fourier spectrum. The spectrum is plotted in Figure 2 and Table 4 details the frequencies found. One-sigma uncertainties are calculated as in Montgomery & Odonoghue (1999). This provides an underestimate of the true uncertainties, but can be used as an indicator of the theoretical limitations of the data.

We removed alias frequencies from the identifications. This includes  $f_7$  which was a  $2\text{d}^{-1}$  alias of  $f_3$ . It is noted that  $f_5$  is identified as a combination frequency in Tarrant et al. (2008), equivalent to the sum of their  $f_2 = 1.36351\text{d}^{-1}$  and  $f_3 = 1.39\text{d}^{-1}$ . There was no evidence for a frequency similar to their  $f_5$  in the present data, yet the  $f_5$  frequency is very close to double the high amplitude frequency  $f_1$ . This means it is probably a harmonic frequency.

We examined the amplitude and phase diagrams of the

**Table 4.** Frequencies found in the analysis of  $\gamma$  Doradus. The spectroscopic frequency  $f_3$  is identified as a one-day alias of the  $1.32 \text{ d}^{-1}$  frequency. The PBP amplitude is measured in normalised intensity units. Sig is the dimensionless spectral significance as described in the text.

ID	Spect.		Phot.		V Amp	Previous work		
	Freq ( $\text{d}^{-1}$ )	PBP Amp	Freq ( $\text{d}^{-1}$ )	Sig		Phot. <sup>1</sup> ( $\text{d}^{-1}$ )	Spec. <sup>2</sup> ( $\text{d}^{-1}$ )	Phot. <sup>3</sup> ( $\text{d}^{-1}$ )
$f_1$	1.3641(2)	0.41	1.36353(2)	99	1.00	1.36354	1.365	1.36351
$f_2$	1.8783(3)	0.25	1.87828(5)	15	0.27			1.87
$f_3$	0.3167(2)	0.35	1.32094(2)	109	0.96	1.32098		1.32093
$f_4$	1.4712(3)	0.22	1.47141(3)	46	0.51	1.475		1.471
$f_5$	2.7428(2)	0.33						
$f_6$	0.0934(2)	0.28	0.91226(5)	18	0.25			
$f_7$	2.3222(3)	0.22						
$f_8$	2.7924(4)	0.16						
$f_9$	4.2471(5)	0.15						
$f_{10}$	2.5876(5)	0.13	2.56369(5)	15	0.18			

<sup>1</sup> Balona et al. (1994a), <sup>2</sup>Balona et al. (1996), <sup>3</sup>Tarrant et al. (2008)

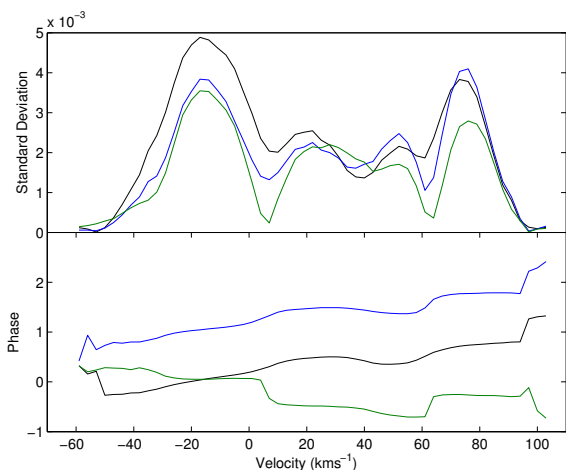


**Figure 3.** Comparison of the standard deviation and phase profiles of  $f_3 = 0.3167 \text{ d}^{-1}$  (black),  $f_3 + 1 \text{ d}^{-1}$  (blue) and  $1.32098 \text{ d}^{-1}$  (green).

PBP identified frequencies in FAMIAS to assist in the detection of further alias frequencies. The frequency  $f_3$  is close to a one day alias of previously detected photometric frequency  $1.32098 \text{ d}^{-1}$ . The standard deviation profile of  $1.32098 \text{ d}^{-1}$  is shown with that of the identified  $f_3$  in Figure 3 and shows a much more symmetric and smooth variation, as well as much more distinct phase changes. We thus adopted the value of  $1.32098 \text{ d}^{-1}$  for  $f_3$  in further analysis.

We noted the two primary frequencies,  $f_1$  and  $f_3$  were similar and thus we further examined them to identify any co-dependence. To determine if  $f_3$  could arise from the identification of  $f_1$  in this particular dataset a synthetic dataset was created. The synthetic data were monophasic and sampled identically to the observations. As only one frequency was inserted, the Fourier spectrum of these synthetic data shows the frequency convolved with the spectral window of the observations. The removal of the identified frequency did not show any residual power in this region. The frequency  $f_3$  is thus unlikely to be an artefact frequency caused by  $f_1$ .

## 4.2 Photometric Frequency Analysis

We analysed a total of 1329  $V$ -band observations from Cousins (1992), Balona et al. (1994a), Balona et al. (1994b) and Balona et al. (1996). These were used to identify frequencies using a very long timespan of 4785 days, more than 13 years. A observation log of all the photometry of  $\gamma$  Doradus is shown in Table 3. Although many of the datasets collected were multi-colour photometry this section restricts analysis to that of the  $V$ -filter as this filter provides the largest number of observations.

We analysed the  $V$ -magnitudes of the photometry in SigSpec for frequencies and the results are shown in Table 4. We discarded alias frequencies. The spectral significance of each frequency is shown in column five of Table 4. Spectral significance is a weighting of the detected frequencies and includes the analysis of the false-alarm probability to remove frequency peaks caused by irregular data sampling or noise in the data (Reegen 2007). We calculated uncertainties in the frequencies as in Kallinger et al. (2008).

## 4.3 Frequency Results

We extracted the frequencies that occurred in photometry and spectroscopy, giving ten candidate pulsation frequencies. We examined each of these frequencies to combine the results. Frequencies  $f_5$  and  $f_7$  have already been discussed as being harmonic and alias frequencies, respectively.

The frequency  $f_6$  appears in several techniques as either  $0.91 \text{ d}^{-1}$  or the  $1 - f$  alias,  $0.09 \text{ d}^{-1}$ . The shape of the standard deviation and phase appears reasonable for a pulsation but has asymmetric amplitudes in the standard deviation profile. Regardless of the shape, a frequency lower than about  $0.3 \text{ d}^{-1}$  is not expected to be found in a  $\gamma$  Dor star unless a mode is retrograde, so we also examined the one-day alias frequencies  $1.0934 \text{ d}^{-1}$  and  $0.9123 \text{ d}^{-1}$ . Both the frequencies had reasonable standard deviation profiles so this frequency remained a candidate for further analysis.

Frequencies  $f_8$ ,  $f_9$  and  $f_{10}$  have low amplitudes, unsymmetric standard deviation profiles and likely arise from combinations of lower frequencies (e.g.  $f_8 = f_3 + f_4$ ) so were not considered further.

To prepare the frequencies for mode-identification, we calculated a least squares fit of all the frequencies together. This process dramatically improved the symmetry of the standard deviation profiles of the frequencies  $f_1$  to  $f_4$ . The last frequency,  $f_6$  was however severely distorted for both the  $0.9123 \text{ d}^{-1}$  and the  $1.0934 \text{ d}^{-1}$  frequencies. This led us to the conclusion that the frequency, although having a reasonable standard deviation profile on its own, must be closely related on one or more of  $f_1$  to  $f_4$  and thus not independent. We therefore did not consider it further in the mode identification and discounted it as a pulsation frequency.

We checked for any characteristic frequency or period spacings between the frequencies  $f_1$  to  $f_4$ . No common spacings could be attributed to the physical properties of the star.

We performed mode identification of the first four frequencies using the spectroscopic identifications for  $f_1$ ,  $f_2$  and  $f_4$  and the photometric identification of the value for  $f_3$  due to the improved standard deviation profile.

## 5 MODE IDENTIFICATION

The spectroscopic mode identification showed multiple well-fitting modes. This led us to use the photometric data to constrain  $l$  and thus differentiate the best modes in spectroscopy. The photometric mode identification is discussed first in Section 5.1 and then informs the spectroscopic analysis in Section 5.2.

### 5.1 Photometric Mode Identification

The largest multi-colour photometry set of the full photometric dataset was taken in the Strömgren filters in 1993 and 1994. The two observing runs yielded a total of 428 observations in the four filters.

We used FAMIAS to identify or constrain the modes of the frequencies  $f_1$  to  $f_4$ . We chose stellar parameters of  $T_{\text{eff}} = 7100 \pm 150 \text{ K}$  and  $\log g = 4.0 \pm 0.2$  as being representative of most of the values found in the literature (see Table 1). The mass was modelled using  $1.8 M_{\odot}$  using the non-adiabatic Warsaw-New Jersey/Dziembowski code<sup>1</sup>. The metallicity was modelled as solar and the microturbulence calculated as  $2 \text{ km s}^{-1}$ . Both the amplitude ratios and the phase differences were tested for  $l = 1$  to  $l = 5$  for all the four frequencies. The results are summarised in Table 5.

The closest fits for the amplitude ratios of  $f_1$  to  $f_4$  were to  $l = 1$ . An example of the amplitude ratio fit to  $f_1$  is given in Figure 4. The phase differences place almost no restrictions on the modes. These results significantly constrain the spectroscopic mode identification in the following section.

<sup>1</sup> Grids of atmospheric parameters have been computed by Leszek Kowalczyk and Jagoda Daszynska-Daszakiewicz (<http://helas.astro.uni.wroc.pl/deliverables.php>) using Kurucz and NEMO atmospheres. Pulsational grid for main-sequence stars with 1.8 to 12 M(sun) computed by Jagoda Daszynska-Daszakiewicz, Alosha Pamyatnykh, and Tomasz Zdravkov using the non-adiabatic Warsaw-New Jersey/Dziembowski code. <http://helas.astro.uni.wroc.pl/deliverables.php?active=opalmodel&lang=en>

**Table 5.** Mode degrees,  $l$ , that fit the amplitude ratios and phase differences of the Strömgren photometric filters.

Filter	$f_1$	$f_2$	$f_3$	$f_4$
Amplitude Ratio				
$A(v)/A(u)$	1	all	-	-
$A(b)/A(u)$	1	all	-	-
$A(y)/A(u)$	4	all	4	4
Phase Difference				
$P(v - u)$	all	all	all	1,3,4,5
$P(b - u)$	all	all	all	all
$P(y - u)$	all	all	all	all

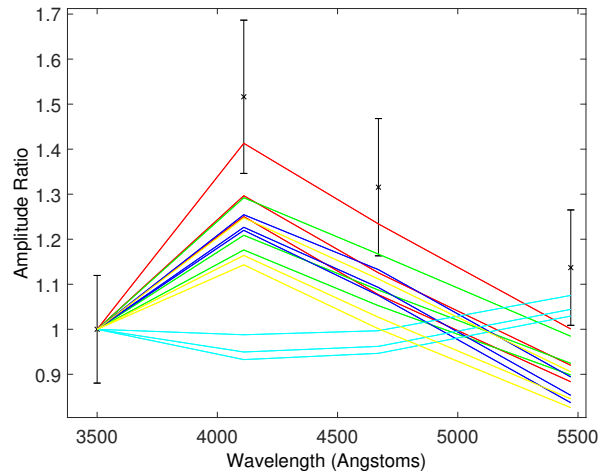


**Figure 4.** Amplitude ratios for the mode identification of  $f_1$ . The colours show the models of different degree, specifically  $l = 1$  (red),  $l = 2$  (green),  $l = 3$  (blue),  $l = 4$  (cyan),  $l = 5$  (yellow). Although a unique solution is not obtained, the results favour the  $l = 1$  mode.

### 5.2 Spectroscopic Mode Identification

We modelled the frequencies found in FAMIAS to determine the best fitting mode. It was noted in the analysis that the standard deviation profiles were shifted such that the centre of the symmetric deviations was translated from the centre of the line profile. The asymmetry of the pulsational distortion of the line profile results in poorer fits for the modes but is not expected to affect the overall identification. This restricts the identification to only using the Amplitude and Phase (AP) fits and not considering the Zero-point, Amplitude and Phase (ZAP) fit in FAMIAS. This is usual practice for the fitting of g-modes, as the zero-point profile fit can statistically dominate over the standard deviation and phase fits and is generally poorer at distinguishing modes.

#### 5.2.1 Line Profile Parameters

We fitted the zero-point profile to measure  $v \sin i$ , equivalent width and velocity offset. The parameters mass, radius and inclination were also permitted to vary. The values for mass and radius are used to determine the horizontal-to-vertical amplitude ratio,  $k$ , and the values do not otherwise affect the

**Table 6.** Line-profile parameters found in the zero-point fit. The minimum  $\chi^2$  value was 489. Non-physical values of radius and mass are discussed in the text.

$\chi^2$	Radius ( $R_\odot$ )	Mass ( $M_\odot$ )	$i$ ( $^\circ$ )	$v \sin i$ ( $\text{km s}^{-1}$ )	Equiv. Width.	avg vel. ( $\text{km s}^{-1}$ )
489	7.51	2.37	9.02	$56.6 (\pm 0.5)$	8.94	22.9

mode-identification. Unrealistic values for mass and radius can arise when fitting a g-mode, which has mostly horizontal motion, with models designed for p-modes, which have mostly vertical motion. The geometric shape of the pulsation ( $l, m$ ) is independent of amplitude in the fits.

The best fit model had a  $\chi^2$  of 489. It is expected that zero-point fits will have high  $\chi^2$  values as they have the lowest measurement uncertainties, thus requiring more precise  $\chi^2$  fits for a lower  $\chi^2$  value. These uncertainties do not reflect all the natural uncertainties in the acquisition and reduction processes but are suitable to be used to judge the best fit profile. The model found with the best-fit values for the parameters is detailed in Table 6.

From the zero-point fit we derived a  $v \sin i$  of  $56.6 \pm 0.5 \text{ km s}^{-1}$ . The uncertainties are from a 95% confidence limit calculated from the critical values of the  $\chi^2$  distribution added to the minimum  $\chi^2$  value.

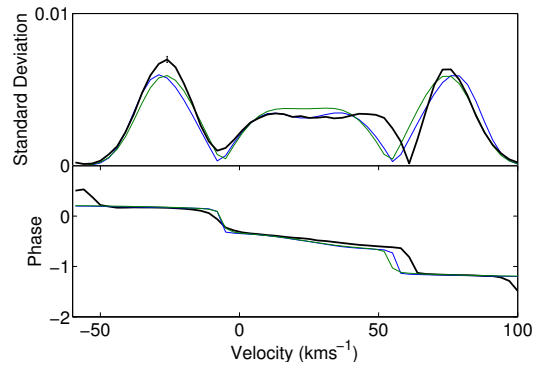
### 5.2.2 Individual Mode Identification

We performed mode identification on each of the frequencies  $f_1$  to  $f_4$  individually. This is done to constrain the parameter space for the simultaneous mode fit. We found a (1, 1) mode best fit frequencies  $f_1$ ,  $f_2$  and  $f_3$ , but  $f_4$  was best fit using a (1, 1), (2, 0) or (2, -2) mode (Figure 5). To further restrict the parameter space to physical regions, we investigated the rotation and pulsation limits of the models.

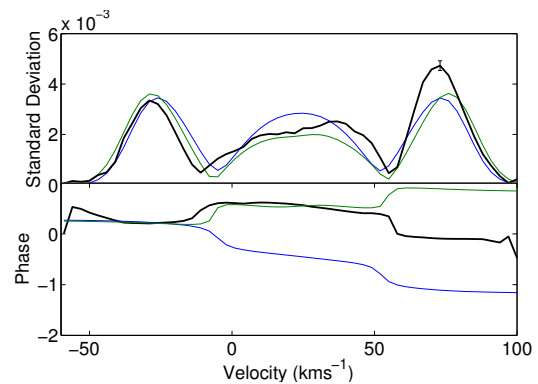
We trialed the frequencies identified for typical  $\gamma$  Dor parameters,  $M = 1.6 M_\odot$  and  $R = 1.5 R_\odot$ , which showed that all the modelled combinations were physically possible except for (1, 1) and (2, 2) modes identified for  $f_3$ . For the (1, 1) mode, the minimum possible inclination of the star which produces a real frequency is  $40^\circ$ . The (2, 2) mode, on the other hand, is not physically possible for any value of  $i$  and is excluded from future consideration for this frequency.

FAMIAS has a general operating limit of  $\frac{f_{rot}}{f_{pul}} < 0.5$ . Fourteen models had individual fits that were higher than this limit. However, none of them were excluded on this principle alone. Most are only slightly greater than 0.5 and low values of  $m$  are less affected by the rotational limit. Lower inclinations increase the  $\frac{f_{rot}}{f_{pul}}$  ratio. For most of the above modes, restricting the inclination removes the risk of producing non-physical models.

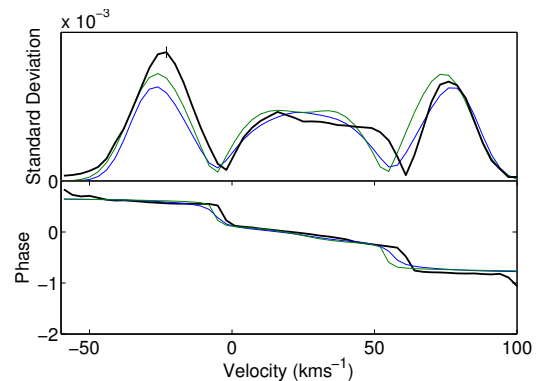
We used typical solutions for  $v \sin i$  and inclination from the individual mode fits, and mass and radius as described above, to determine an estimate of the equatorial rotational velocity, rotation frequency and critical limits of  $v \sin i$  and inclination when stellar break-up occurs. A  $v \sin i \approx 57 \text{ km s}^{-1}$  and  $i \approx 60^\circ$  corresponds to a star with an equatorial rotation velocity of around  $66 \text{ km s}^{-1}$ , and rotational frequency of approximately  $0.9 \text{ d}^{-1}$ . To exceed



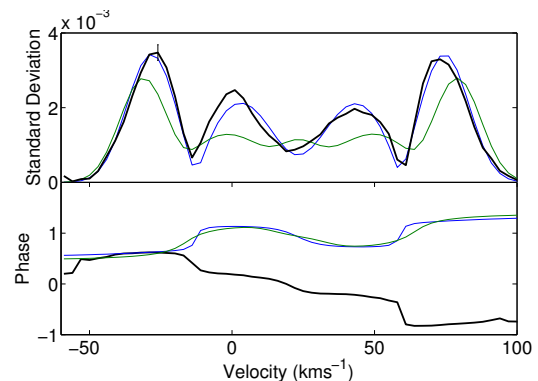
(a)  $f_1 = 1.3641 \text{ d}^{-1}$  with a (1, 1) mode ( $\chi^2 = 10.6$ ).



(b)  $f_2 = 1.8783 \text{ d}^{-1}$  with a (1, 1) mode ( $\chi^2 = 3.88$ ).



(c)  $f_3 = 1.3209 \text{ d}^{-1}$  with a (1, 1) mode ( $\chi^2 = 11.8$ ).



(d)  $f_4 = 1.4742 \text{ d}^{-1}$  with a (2, 0) mode (blue,  $\chi^2 = 2.6$ ) and a (2, -2) mode (green,  $\chi^2 = 6.4$ ).

**Figure 5.** Mode identification of the four identified frequencies. The standard deviation and phase profiles (black) with the individual fits (blue) and combined fit (green) are shown for the four identified frequencies. The combined fit has a  $\chi^2$  of 14.2. An

**Table 7.** Best fit parameters for a multi-mode parameter search using  $f_1$  to  $f_3$  and allowing the mode of  $f_4$  to vary. Velocity amplitudes (Vel.) are in units of  $\text{km s}^{-1}$ . Models with  $\chi^2$  less than 25 are shown, with other mode fits having much higher  $\chi^2$  ( $> 50$ ).

$\chi^2$	$R$ ( $R_\odot$ )	$M$ ( $M_\odot$ )	$i$ ( $^\circ$ )	$v \sin i$ ( $\text{km s}^{-1}$ )	avg. Vel. ( $\text{km s}^{-1}$ )	$f_1$		$f_2$		$f_3$		$f_4$			
						Vel.	Ph.	Vel.	Ph.	Vel.	Ph.	Vel.	Ph.	$l_{f_4}$	$m_{f_4}$
14.2	3.87	5.21	31.9	58.4	24	2	0.76	2.7	0.8	3.86	0.68	1.3	0.19	2	-2
14.8	4.31	7.23	30	59.9	24	2	0.76	2.7	0.8	1.03	0.17	1.3	0.18	1	1
18.6	3.87	5.21	30	59.6	24.7	2	0.75	2.7	0.8	0.01	0.2	1.3	0.17	2	2
20.3	4.39	7.91	30	59.6	24	2	0.76	2.7	0.8	0.8	0.68	1.3	0.19	3	-2
21.5	4.17	6.48	30	59.4	24.7	2	0.75	2.7	0.8	0.4	0.66	1.3	0.18	2	-1
21.5	4.24	6.86	30	59.9	24	2	0.76	2.7	0.8	1.35	0.62	1.3	0.18	0	0
22.1	4.09	6.19	30	59.2	24.7	2	0.75	2.7	0.8	0.25	0.91	1.3	0.18	3	-3
22.3	4.39	7.68	30	59.6	24	2	0.76	2.7	0.8	0.48	0.51	1.3	0.18	1	-1

break-up velocity the critical  $v \sin i$  is  $390 \text{ km s}^{-1}$  and critical minimum inclination of  $7^\circ$ . Models with inclination of less than  $7^\circ$  were thus rejected. The star is not otherwise close to rotating near the break-up velocity. A rotational frequency near  $1 \text{ d}^{-1}$  is expected for  $\gamma$  Doradus given the  $v \sin i$ . These values range from around  $1.5 \text{ d}^{-1}$  to  $0.75 \text{ d}^{-1}$  for inclinations in the range of  $30^\circ - 90^\circ$ .

### 5.2.3 Combined Mode Identification

The photometric mode identification suggests a best fit  $l$  value for all the frequencies of  $l = 1$ . The identification of the  $f_1$ ,  $f_2$  and  $f_3$  frequencies can be therefore concluded to be (1, 1) modes from the best fits in the individual mode analysis. The identification of  $f_4$  is more complex. The mode (2, 2) must first be excluded as it has already been deemed non-physical. The shape of the (1, 1) mode is also excluded as the best fit model still displays a three-bump structure that does not fit the four bumps observed for this frequency. It is not expected that  $f_4$  should have a much higher velocity amplitude than the other frequencies, thus the identification of the above modes suggests that modes (2, 0), (3, 0) and (2, -2) should be favoured. Since the mass and radius of the star are allowed to vary non-physically, it is prudent to not discard the modes based on the amplitudes alone. The parameter space searched for  $f_4$  included the higher amplitude frequencies with all models with  $l = 2$  and  $l = 3$  considered so as not to miss any possible identifications.

We constrained the inclination to be a minimum of  $30^\circ$ . Inclinations lower than this limit produce very high amplitude intrinsic pulsation frequencies, which are not theoretically predicted for self-excited g-modes in these stars. Additionally, the observational amplitudes of the pulsations and the probability of the existence of an equatorial wave-guide for a rotating, pulsating star make it unlikely that such amplitudes of pulsation could be observed in spectroscopy, and would be nearly impossible to detect in photometry.

We undertook a combined mode-identification search to fit the stellar parameters and to find the best mode fit for  $f_4$  that was consistent with the other frequencies. The best fit models are shown in Table 7 and plotted in Figure 5. Not all the fits in the table should be regarded as accurate fits to the star. The radius and mass parameters have been allowed to vary considerably beyond the physical limits for a  $\gamma$  Dor star in order to produce visible amplitudes of pulsation. Even

with these large values, the velocity amplitudes for most of the fits are much higher than expected.

From these models, and the fits, it is clear that the three frequencies,  $f_1$ ,  $f_2$  and  $f_3$ , are well modelled by (1, 1) modes. The other frequency,  $f_4$ , does not appear to be well modelled by the lowest  $\chi^2$  fit. To see if the fits matched well over the entire phase of each pulsation frequency, we computed synthetic profiles of the frequencies using the modes and parameters determined in the best fit in Table 7. These are compared with the phased line profiles observed in Figure 6 for  $f_1$ ,  $f_2$  and  $f_3$  and Figure 7 for  $f_4$ . The (1, 1) mode frequencies in Figure 6 were all well fitted in phase space and this supports their identification. The two proposed fits for  $f_4$  in Figure 7 are less clear, but it can be seen that the (2, 0) mode better describes the variation over the phase of the frequency, even though it is inconsistent with the best fits for the combined mode identification.

We calculated the co-rotating frequencies of the identifications  $f_1$  to  $f_4$  to identify if the  $l = 2$  identification for  $f_4$  was consistent with the expectation that higher order modes have higher frequencies (Dupret et al. 2005). The co-rotating frequencies were calculated as in Dziembowski & Goode (1992),  $f_{\text{corot}} = f_{\text{obs}} - m(1 - C)f_{\text{rot}}$ , using the parameters of the best fit in Table 7 and  $C = \frac{1}{l(l+1)}$ .

We found the frequencies  $f_1$ ,  $f_2$  and  $f_3$  to have co-rotating frequencies ranging from  $1.0388 \text{ d}^{-1}$  to  $1.5962 \text{ d}^{-1}$ . The co-rotating frequency for  $f_4$  is  $1.4712 \text{ d}^{-1}$  and  $2.4115 \text{ d}^{-1}$  for the (2, 0) and (2, -2) mode respectively. The (2, -2) mode frequency is higher than the  $l = 1$  identifications so this supports the identification of  $f_4$  as a (2, -2) mode, but as these co-rotating frequencies can only be estimated this does not rule out the (2, 0) mode.

Due to the poorness of the fit obtained for  $f_4$ , we also performed the multi-mode fit on just the well-identified frequencies  $f_1$ ,  $f_2$  and  $f_3$ . This produced best fit parameters nearly identical to the combined mode identification with a  $\chi^2$  of 14.0. The difficulties in fitting the four modes simultaneously questions the validity of the  $f_4$  frequency, but there is no other evidence for excluding it as a valid frequency arising from a (2, 0) mode. Parameters usually reported from these fits include the  $v \sin i$  and the inclination. Fitting the zero-point profile above gave a credible  $v \sin i$  and this was not seen to vary significantly in the individual or combined mode fits. Although the best fit inclination was found to be at  $31^\circ$ , this would need to be confirmed using

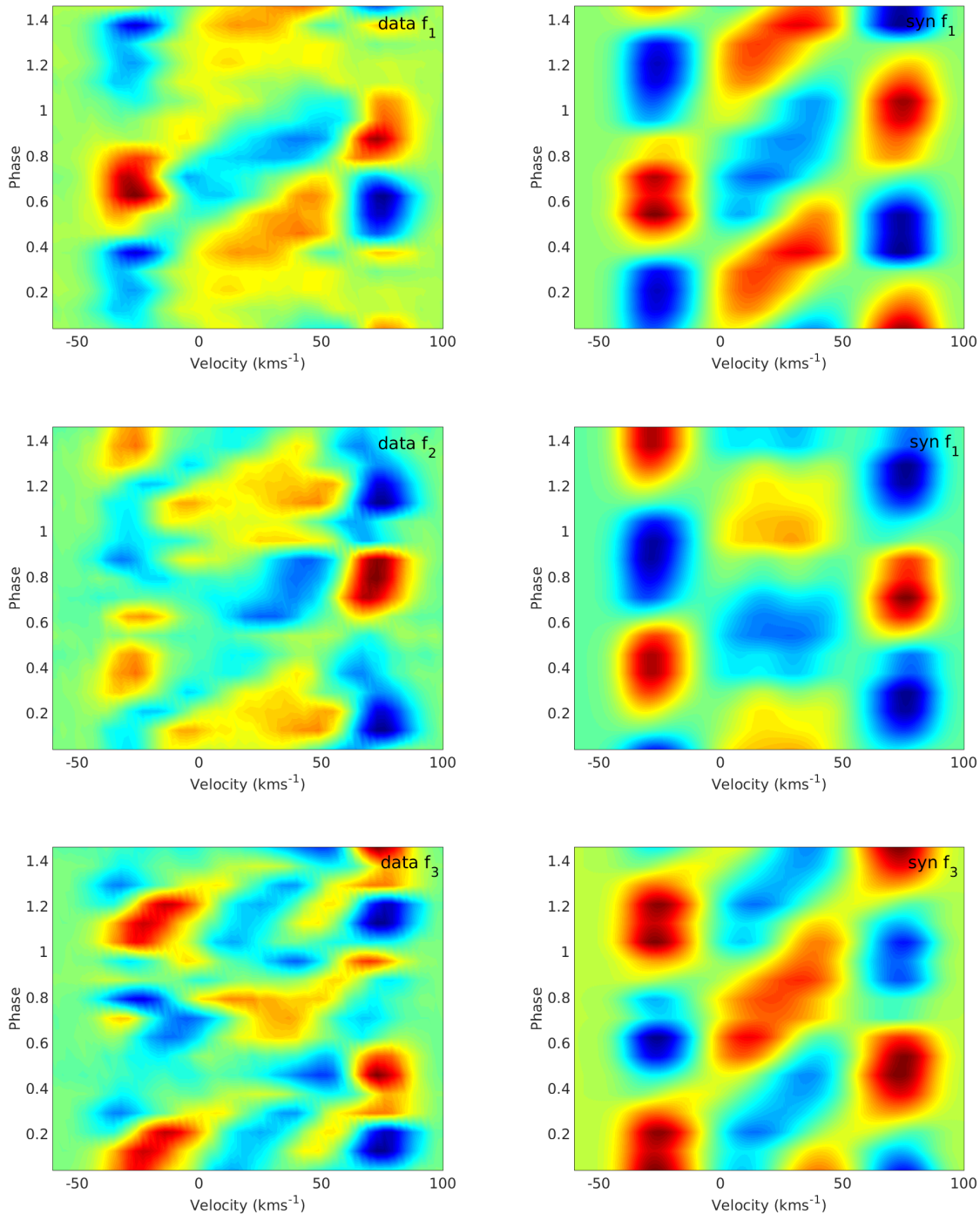


**Figure 6.** Phased residual line profile variations of the observed spectra (left column) and the synthetic models using the combined fit (right column) for frequencies  $f_1$ ,  $f_2$  and  $f_3$ , all fitted with (1, 1) modes.

a model that accounts for all the observed frequencies and modes. Because of the difficulties with the identification of the modes in this star this would likely have to be a model that accounts for the rotation and horizontally-dominated motion of a  $\gamma$  Dor pulsation.

## 6 DISCUSSION

The implications of fitting a non-physical mass and radius in the model are concerning. The mass and radius, along with the other parameters, are all allowed to vary in the individual and combined mode fits. The high values for the velocity amplitudes are an indication of a non-physical fit for a  $\gamma$  Dor star. The amplitude of pulsation alone does not have



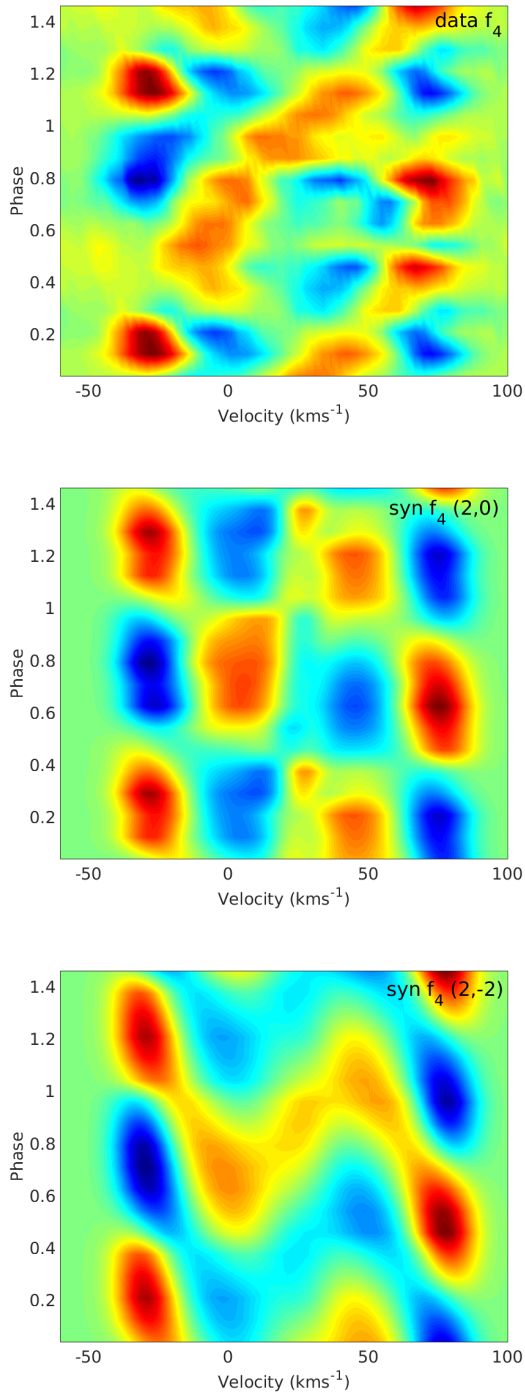


**Figure 7.** Phased residual line profile variations of the observed spectra for  $f_4$  and two models. The first model is the individual frequency fit with mode  $(l, m) = (2, 0)$  and the second model is the combined mode fit with a  $(2, -2)$  mode.

a significant effect on the shape of the line profile. In fact, changing the mass and radius has a much more significant effect on the observed amplitude than the intrinsic velocity amplitude, since this affects the value of  $k$ , the horizontal-vertical amplitude ratio.

The frequencies found in the analysis of  $\gamma$  Doradus are almost identical to those found in previous spectroscopic and

photometric studies. No new frequencies were found but this work confirms the proposal of the frequency at  $1.878 \text{ d}^{-1}$  by Tarrant et al. (2008). The frequencies  $f_1$  and  $f_3$  are shown to be stable over twenty years since their first identification by Cousins (1992). This long-term stability of frequencies is also seen in the  $\gamma$  Dor star HD 108100, (Breger et al. 1997).

$\gamma$  Doradus shows an excellent agreement between the frequencies found in photometry and spectroscopy. This has not always been the case for previously studied  $\gamma$  Dor stars (e.g. Uytterhoeven et al., 2008, Brunsden et al., 2015) although other stars show similar agreement (e.g. Brunsden et al., 2012, Sódor et al., 2014). It is not known why such differences should occur, but this work continues with the complementary data from large photometric surveys and targeted high-resolution spectroscopic campaigns. The power of combining the techniques lies in the precise identification of frequencies from photometry with the two-dimensional information provided from the line profiles.

An investigation into the aliases and combination frequencies led us to remove of the frequency at  $2.74 \text{ d}^{-1}$  as a harmonic of  $f_1$ . Tarrant et al. (2008) also removed this frequency, identifying it as a combination of  $1.36351 \text{ d}^{-1}$  and their proposed  $1.39 \text{ d}^{-1}$ . We found no evidence for a further frequency near  $1.39 \text{ d}^{-1}$  in this analysis. The relationship between the two close frequencies  $f_1$  and  $f_4$  was examined but no evidence for a link between them was discovered.

Balona et al. (1996) found modes of  $(l, m) = (1, 1)$ ,  $(3, 3)$  and  $(1, 1)$  for the frequencies  $f_1$ ,  $f_3$  and  $f_4$  respectively, using spectroscopic line profile variations with further assumptions. Additionally, Dupret et al. (2005) found  $f_1$  and  $f_3$  to be both well-fitted by  $l = 1$  modes. These results confirm the identification of  $(l, m) = (1, 1)$  for  $f_1$ ,  $f_2$  and  $f_3$ . They also give independent confirmation of the robustness of the g-modes detected in FAMIAS, even when the strong horizontal nature of a g-mode pulsation forces the use of non-physical parameters to obtain the fit. The mode identification for  $f_4$  showed a best fit with a  $(2, 0)$  mode but was not consistent with the fits of the other frequencies. Despite this result, the frequency is not discarded as a pulsation frequency. The co-rotating frequencies of the modes found support the identification of  $f_4$  as a higher degree mode than the other frequencies. It is hoped that, with more physically descriptive models of  $\gamma$  Dor stars, this inconsistency will be resolved.

We determined stellar parameters of  $v \sin i$  and inclination in this analysis. The measurement of the zero-point line profile gave a value of  $56.6 \pm 0.5 \text{ km s}^{-1}$  based on a 95% confidence interval. Inclination was best fit to be  $31^\circ$  for a multi-modal fit of the four frequencies. However, this parameter is often not well constrained by mode identification. This compares to the values of Balona et al. (1996) and Broekhoven-Fiene et al. (2013) who found inclination of  $\approx 70^\circ$ . The existence of a debris disc around  $\gamma$  Doradus (Koerner et al. 2010) may help to improve pulsation models by constraining the inclination of the star (assuming the rotation and pulsation axes align with the disc axis). The absence of evidence of disc signatures in the spectra of  $\gamma$  Doradus suggests the disc is sparse across the stellar surface, or potentially does not cross the line-of-sight to the star.

The Transiting Exoplanet Survey Satellite (TESS), expected to be launched in March 2018, will perform a

two-year high-precision time-resolved photometric survey of nearly the entire sky.  $\gamma$  Doradus is proposed<sup>2</sup> to be observed in short-cadence (2 minutes) and is observable for three epochs (Mukai & Barclay 2017) of around 27 days in length. This ultra-precise dataset will provide valuable precision photometric data to align with spectroscopic results.

## 7 CONCLUSION

The study of  $\gamma$  Doradus as the prototype of its class, is important to furthering current understanding of these pulsations. The star's visual brightness and southerly latitude has made it an ideal target for southern hemisphere observers. The multitude of photometric results also allows confirmation of photometric and spectroscopic techniques for these stars. Despite the requirement to go beyond physically possible parameter space in modelling the mass and radius of the star, the mode identification was successful and proves the validity of this technique. It is hoped that using non-physical models will not be necessary with improvements to theoretical models, which will be able to account for rotational effects and be specifically adapted to identify g-modes. The star  $\gamma$  Doradus will be an excellent candidate for testing such models.

## 8 ACKNOWLEDGEMENTS

This work was supported by the Marsden Fund administered by the Royal Society of New Zealand.

The authors acknowledge the assistance of staff at the University of Canterbury's Mt John Observatory.

We appreciate the time allocated at other facilities for multi-site campaigns and the numerous observers who make acquisition of large datasets possible.

This research has made use of the SIMBAD astronomical database operated at the CDS in Strasbourg, France.

Mode identification results obtained with the software package FAMIAS developed in the framework of the FP6 European Coordination action HELAS (<http://www.helas-eu.org/>).

The authors wish to thank L. A. Balona for providing data and discussions regarding this paper.

We are thankful to Simon J. Murphy for helpful comments which improved this manuscript.

## REFERENCES

- Ammler-von Eiff M., Reiners A., 2012, *A&A*, 542, A116  
 Balona L. A., 1986a, *MNRAS*, 219, 111  
 Balona L. A., 1986b, *MNRAS*, 220, 647  
 Balona L. A., 1987, *MNRAS*, 224, 41  
 Balona L. A., Böhm T., Foing B. H., Ghosh K. K., Janot-Pacheco E., Krisciunas K., Lagrange A.-M., Lawson W. A., James S. D., Baudrand J., Catala C., Dreux M., Felenbok P., Hearnshaw J. B., 1996, *MNRAS*, 281, 1315  
 Balona L. A., et al., 1994a, *MNRAS*, 270, 905  
 Balona L. A., et al., 1994b, *MNRAS*, 267, 103  
 Balona L. A., Stobie R. S., 1979, *MNRAS*, 189, 649  
 Bedding T. R., Murphy S. J., Colman I. L., Kurtz D. W., 2015, in *European Physical Journal Web of Conferences* Vol. 101 of *European Physical Journal Web of Conferences*, Échelle diagrams and period spacings of g modes in  $\gamma$  Doradus stars from four years of Kepler observations. p. 01005  
 Breger M., Handler G., Garrido R., Audard N., Beichbuchner F., Zima W., Paparo M., Li Z.-P., Jiang S.-Y., Liu Z.-L., Zhou A.-Y., Pikall H., Stankov A., Guzik J. A., Sperl M., others. 1997, *A&A*, 324, 566  
 Broekhoven-Fiene H., Matthews B. C., Kennedy G. M., Booth M., Sibthorpe B., Lawler S. M., Kavelaars J. J., Wyatt M. C., Qi C., Koning A., Su K. Y. L., Rieke G. H., Wilner D. J., Greaves J. S., 2013, *ApJ*, 762, 52  
 Brunsden E., Pollard K. R., Cottrell P. L., Uytterhoeven K., Wright D. J., De Cat P., 2015, *MNRAS*, 447, 2970  
 Brunsden E., Pollard K. R., Cottrell P. L., Wright D. J., De Cat P., 2012, *MNRAS*, 427, 2512  
 Cousins A. W. J., 1960, *Monthly Notes of the Astronomical Society of South Africa*, 19, 56  
 Cousins A. W. J., 1992, *The Observatory*, 112, 53  
 Cousins A. W. J., Warren P. R., 1963, *Monthly Notes of the Astronomical Society of South Africa*, 22, 65  
 Cugier H., Dziembowski W. A., Pamyatnykh A. A., 1994, *A&A*, 291, 143  
 Daszyńska-Daszkiewicz J., Dziembowski W. A., Pamyatnykh A. A., Goupil M.-J., 2002, *A&A*, 392, 151  
 Dupret M.-A., De Ridder J., De Cat P., Aerts C., Scuflaire R., Noels A., Thoul A., 2003, *A&A*, 398, 677  
 Dupret M.-A., Grigahcène A., Garrido R., De Ridder J., Scuflaire R., Gabriel M., 2005, *MNRAS*, 360, 1143  
 Dupret M.-A., Grigahcène A., Garrido R., Gabriel M., Scuflaire R., 2005, *A&A*, 435, 927  
 Dziembowski W. A., Goode P. R., 1992, *ApJ*, 394, 670  
 Grassitelli L., Fossati L., Langer N., Miglio A., Istrate A. G., Sanyal D., 2015, *A&A*, 584, L2  
 Gray R. O., Corbally C. J., Garrison R. F., McFadden M. T., Bubar E. J., McGahee C. E., O'Donoghue A. A., Knox E. R., 2006, *AJ*, 132, 161  
 Guzik J. A., Kaye A. B., Bradley P. A., Cox A. N., Neuforge C., 2000, *ApJ*, 542, L57  
 Hearnshaw J. B., Barnes S. I., Kershaw G. M., Frost N., Graham G., Ritchie R., Nankivell G. R., 2002, *Experimental Astronomy*, 13, 59  
 Hubeny I., Lanz T., 2011, *Astrophysics Source Code Library*, p. 9022  
 Kahraman A. İ., Niemczura E., Polińska M., Helminiak K. G., Lampens P., Molenda-Żakowicz J., Ukita N., Kambe E., 2017, *MNRAS*, 470, 4408  
 Kallinger T., Reegen P., Weiss W. W., 2008, *A&A*, 481, 571  
 Kaye A. B., Handler G., Krisciunas K., Poretti E., Zerbi F. M., 1999, *PASP*, 111, 840  
 Koerner D. W., Kim S., Trilling D. E., Larson H., Cotera A., Stapelfeldt K. R., Wahhaj Z., Fajardo-Acosta S., Padgett D., Backman D., 2010, *ApJL*, 710, L26  
 Mantegazza L., 2000, in M. Breger & M. Montgomery ed., *Delta Scuti and Related Stars* Vol. 210 of *Astronomical Society of the Pacific Conference Series*, Mode Detection

<sup>2</sup> <https://tasoc.dk/info/targetlist.php>

- from Line-Profile Variations. p. 138
- Montgomery M. H., Odonoghue D., 1999, Delta Scuti Star Newsletter, 13, 28
- Mukai K., Barclay T., 2017, tvguide: A tool for determining whether stars and galaxies are observable by TESS, v1.0.0
- Reegen P., 2007, A&A, 467, 1353
- Schmid V. S., Aerts C., 2016, A&A, 592, A116
- Sódor Á., Chené A.-N., De Cat P., Bognár Z., Wright D. J., Marois C., Walker G. A. H., Matthews J. M., Kallinger T., Rowe J. F., Kuschnig R., Guenther D. B., Moffat A. F. J., Rucinski S. M., Sasselov D., Weiss W. W., 2014, A&A, 568, A106
- Sokolov N. A., 1995, A&AS, 110, 553
- Tarrant N. J., Chaplin W. J., Elsworth Y. P., Sreckley S. A., Stevens I. R., 2008, A&A, 492, 167
- Uytterhoeven K., Mathias P., Poretti E., Rainer M., Martín-Ruiz S., Rodríguez E. and Amado P. J., Le Contel D., Jankov S., Niemczura E., Pollard K. R., Brunsten E., Paparó M., Costa V., et al., 2008, A&A, 489, 1213
- Van Reeth T., Tkachenko A., Aerts C., 2016, A&A, 593, A120
- Watson R. D., 1988, Ap&SS, 140, 255
- Wright D. J., 2008, PhD thesis, University of Canterbury
- Wright D. J., Pollard K. R., Cottrell P. L., 2007, Communications in Asteroseismology, 150, 135
- Xiong D. R., Deng L., Zhang C., Wang K., 2016, MNRAS, 457, 3163
- Zima W., 2008, Communications in Asteroseismology, 157, 387
- Zima W., 2009, A&A, 497, 827
- Zima W., Wright D., Bentley J., Cottrell P. L., Heiter U., Mathias P., Poretti E., Lehmann H., Montemayor T. J., Breger M., 2006, A&A, 455, 235